Structure of Tetrahydrobiopterin Tunes its Electron Transfer to the Heme−Dioxy Intermediate in Nitric Oxide Synthase†

Chin-Chuan Wei,‡ Zhi-Qiang Wang,‡ Andrew S. Arvai,§ Craig Hemann,|| Russ Hille,|| Elizabeth D. Getzoff,§ and Dennis J. Stuehr*,‡

Department of Immunology, The Lerner Research Institute, Cleveland Clinic Foundation, Cleveland, Ohio 44195, Department of Molecular Biology, The Skaggs Institute for Chemical Biology, The Scripps Research Institute, La Jolla, California 92037, and Department of Molecular and Cellular Biochemistry, Ohio State University, Columbus, Ohio 43210

Received September 25, 2002; Revised Manuscript Received December 29, 2002

ABSTRACT: How 6*R*-tetrahydrobiopterin (H_4B) participates in Arg hydroxylation as catalyzed by the nitric oxide synthases (NOSs) is a topic of current interest. Previous work with the oxygenase domain of inducible NOS (iNOSoxy) demonstrated that H_4B radical formation is kinetically coupled to disappearance of an initial heme−dioxy intermediate and to Arg hydroxylation in a single turnover reaction run at 10 °C [Wei, C.-C., Wang, Z.-Q., Wang, Q., Meade, A. L., Hemann, C., Hille, R., and Stuehr, D. J. (2001) *J. Biol. Chem. 276*, 315−319]. Here we used 5-methyl-H_4B to investigate how pterin structure influences radical formation and associated catalytic steps. In the presence of Arg, the heme−dioxy intermediate in 5-methyl-H_4B-bound iNOSoxy reacted at a rate of 35 s^{-1}, which is 3-fold faster than with H_4B. This was coupled to a faster rate of 5-methyl-H_4B radical formation (40 vs 12.5 s^{-1}) and to a faster and more productive Arg hydroxylation. The EPR spectrum of the enzyme-bound 5-methyl-H_4B radical had different hyperfine structure than the bound H_4B radical and exhibited a 3-fold longer half-life after its formation. A crystal structure of 5-methyl-H_4B-bound iNOSoxy revealed that there are minimal changes in conformation of the bound pterin or in its interactions with the protein as compared to H_4B. Together, we conclude the following: (1) The rate of heme−dioxy reduction is linked to pterin radical formation and is sensitive to pterin structure. (2) Faster heme−dioxy reduction increases the efficiency of Arg hydroxylation but still remains rate limiting for the reaction. (3) The 5-methyl group influences heme−dioxy reduction by altering the electronic properties of the pterin rather than changing protein structure or interactions. (4) Faster electron transfer from 5-methyl-H_4B may be due to increased radical stability afforded by the N-5 methyl group.

Nitric oxide synthases (NOSs[1], EC 1.14.13.39) are flavoheme enzymes that catalyze oxidation of L-arginine (Arg) to nitric oxide (NO) and L-citrulline (*1*−*3*). The reaction is catalyzed in two steps with the first being a NADPH- and O_2-dependent hydroxylation of Arg that forms N^G-hydroxyl-L-arginine (NOHA) as an enzyme-bound intermediate (Scheme 1). Reactions take place within a heme-containing oxygenase domain dimer (NOSoxy) that receives electrons from attached flavoprotein domains. NOSoxy proteins can be expressed independently and can catalyze both steps of NO synthesis if provided with a source of electrons (*4*−*6*).

Scheme 1: Reaction Catalyzed by NO Synthases

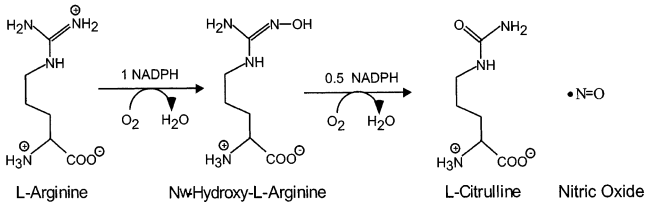

NOS are unique among flavoheme enzymes because they contain (6*R*)-5,6,7,8-tetrahydro-L-biopterin (H_4B) as a tightly bound cofactor. Crystal structures of various NOSoxy proteins revealed how heme, Arg, and H_4B bind within the active site and have identified residues that interact with H_4B (*7*−*9*). How H_4B and heme cooperate during oxygen activation is a topic of current interest. The NOS ferric heme receives an electron from the flavoprotein domain, and this step limits the rate of NO synthesis in the full-length enzyme (*10*−*12*). Dioxygen then binds to ferrous heme to create a heme−dioxy intermediate ($Fe^{III}O_2^-$) that has been directly observed in NOS and characterized by various spectroscopic methods (*4*, *13*−*16*). The $Fe^{III}O_2^-$ species must receive another electron to complete the oxygen activation process. Although the NOS flavoprotein can supply this electron (*17*,

† This work was supported by National Institutes of Health Grants CA53914 (D.J.S.), HL 58883 (E.D.G.), and GM58481 (R.H.) and by a Fellowship from the American Heart Association (C.-C.W.).

* To whom correspondence should be addressed. Tel: (216) 445-6950. Fax: (216) 444-9329. E-mail: stuehrd@ccf.org.

‡ Lerner Research Institute.

§ The Scripps Research Institute.

|| The Ohio State University.

[1] Abbreviations: NO, nitric oxide; NOS, nitric oxide synthase; NOSoxy, NOS oxygenase domain; NOHA, N^G-hydroxyl-L-arginine; H_4B, (6*R*)-5,6,7,8-tetrahydro-L-biopterin; 5MeH_4B, (6*R*)-5-methyl-6,7,8-trihydro-L-biopterin; iNOSoxy, mouse inducible NOS oxygenase domain; $Fe^{III}O_2^-$, heme ferric superoxy intermediate; EPPS, *N*-(2-hydroxyethyl)-piperazine-*N*′-3-propanesulfonic acid; MES, 2-(*N*-morpholino)ethanesulfonic acid; BOG, *N*-octyl-*β*-D-glucopyranoside.

10.1021/bi026898h CCC: $25.00
Published on Web 01/31/2003

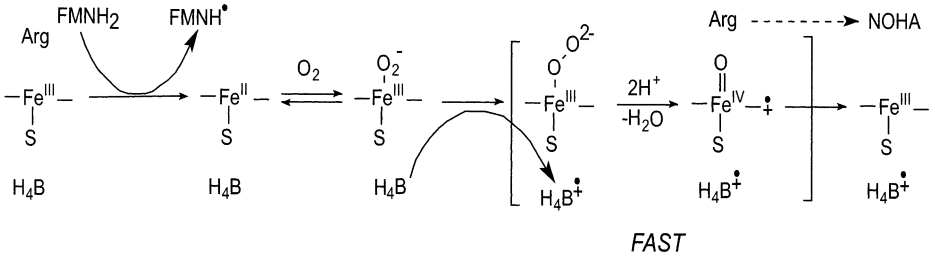

FIGURE 1: Model of Arg hydroxylation. In an NADPH-driven reaction, the slow step is electron transfer from the NOS flavoprotein ($FMNH_2$) to the ferric heme. Dioxygen then binds to the ferrous heme to form the $Fe^{III}O_2^-$ species, which receives an electron from H_4B and forms a presumed heme−peroxo intermediate that was recently characterized spectroscopically (*49*). Subsequent steps that lead to and include Arg hydroxylation are as fast or faster than H_4B electron transfer. The reaction generates ferric iNOSoxy containing NOHA and the H_4B radical. Adapted from ref *19*.

18), H_4B is a kinetically preferred source when it is bound (*19*−*21*). H_4B reduction of the $Fe^{III}O_2^-$ intermediate has been studied in single turnover Arg hydroxylation reactions catalyzed by NOSoxy proteins (*15*, *19*, *21*−*23*). The resulting H_4B radical appears to be cationic (*23*) and exists long enough in NOSoxy so that its buildup and decay can be investigated by rapid freezing and EPR spectroscopy (*19*, *21*, *22*).

Our single turnover studies of Arg hydroxylation in mouse inducible NOSoxy (iNOSoxy) showed that reduction of the $Fe^{III}O_2^-$ intermediate by H_4B is kinetically coupled to Arg hydroxylation (*19*) (Figure 1). Moreover, a conserved Trp residue (W457) that interacts with H_4B by π stacking was found to control the tempo of $Fe^{III}O_2^-$ reduction by H_4B (*22*). This appears important because slower reduction of $Fe^{III}O_2^-$ by H_4B in the mutants was associated with slower and less complete Arg hydroxylation. Crystal structures of the W457 iNOSoxy mutants suggest that they alter H_4B redox function by causing discreet structural changes within iNOSoxy that destabilize the H_4B radical cation (*24*). Thus, it appears that the iNOSoxy protein can influence the tempo of $Fe^{III}O_2^-$ reduction by H_4B and in this way control the extent of Arg hydroxylation.

Given the above, we investigated if altering H_4B structure would influence its redox function during Arg hydroxylation in the single turnover system. Several structural analogues of H_4B are known to bind to NOS and support either full or diminished NO synthesis rates as compared to H_4B (*25*−*27*). In particular, the N^5-methyl analogue of H_4B ($5MeH_4B$) was found to support full NO synthesis by neuronal NOS (*25*). We chose this analogue for our current study, reasoning that the N5 methyl group might affect radical formation or stability during Arg hydroxylation. We determined the kinetics of heme transitions, radical formation and decay, and Arg hydroxylation in a single catalytic turnover by $5MeH_4B$-containing iNOSoxy and solved a crystal structure of the $5MeH_4B$-bound protein to 1.8 Å resolution. The kinetic differences, their possible structural basis, and mechanistic implications are presented and discussed.

MATERIALS AND METHODS

Chemicals. [U-^{14}C]Arg was purchased from Perkin-Elmer Life Sciences. $5MeH_4B$ was obtained from Schircks Laboratory (Jona, Switzerland). All other chemicals were obtained either from Sigma Chemical Company or Fisher Scientific.

Protein Expression and Purification. Mouse iNOSoxy (amino acid 1−498) containing a six-histidine tag at the C-terminus was expressed in *Escherichia coli* BL21 using the PCW*ori* vector and purified in the absence of H_4B as reported previously (*28*). The enzyme concentration was determined from the 444 nm absorbance of the ferrous−CO complex by using an extinction coefficient of 76 mM^{-1} cm^{-1}. The concentrated protein was diluted in buffer containing 50 mM HEPES (pH 7.5), 2 mM β-mercaptoethanol, and 0.25 M NaCl before use.

UV−*Vis Spectrometry.* Conventional spectra were obtained using a Cary 100 BIO instrument equipped with temperature control and automatic stirring.

Kinetic Experiments. Ferrous iNOSoxy was prepared as described previously (*19*). Prior to performing the dithionite titration, a solution containing concentrated iNOSoxy, 1 or 2 mM $5MeH_4B$, and 10 or 20 mM Arg was incubated overnight for the stopped-flow and rapid-freeze experiments, respectively. All single turnover reactions were performed at 10 °C. The rapid-scanning stopped-flow spectroscopy, rapid-quench experiment, amino acid HPLC analysis, and rapid-freeze EPR were performed as described previously (*19*). Experiments were repeated at least three times for stopped-flow and rapid-quench experiments and two times for the rapid-freeze EPR experiment. The protein concentrations and reaction conditions are described in the text.

Analysis of EPR Data. Kinetics of radical formation and decay and the amount of radical formed per heme were determined using methods described previously (*19*). The $p_{1/2}$ value of microwave power saturation for the $5MeH_4B$ radical was determined over a microwave power range of 50.2 μW to 200 mW and utilized least-squares fitting. Simulations of EPR spectra were carried out using the XEMR simulation package (*50*), operating under the Linux operating system. A simple $S = 1/2$ system was assumed, with isotropic **g** and **A** tensors. Satisfactory simulations were obtained assuming coincident tensors (i.e., with Euler *q* and *f* angles of 0. The linewidths providing the best fits for the spectra for H_4B and 5-Me H_4B were 8.5 and 7 G, respectively, along with a Laurentzian/Gaussian line shape ratio of 1.0 in each case.

Stoichiometry Measurement. The amount of NOHA formed per heme from Arg in the single turnover reaction was determined by HPLC with precolumn derivatization or with radioisotope detection. Briefly, 0.1 mM iNOSoxy was incubated with 1 mM $5MeH_4B$ or H_4B and 1, 3, or 6 mM Arg. The solution was made anaerobic, the enzyme reduced by dithionite titration, and then 0.2 mL of the solution was mixed with 50 μL of O_2-saturated buffer. The reaction sample was then stored in a mixture of ethanol and dry ice. HPLC detection was performed as described using orthophalalde-

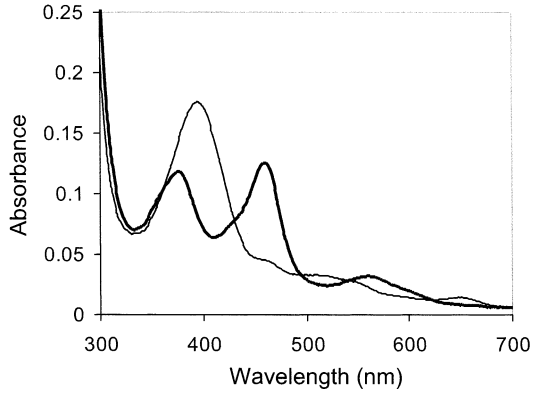

FIGURE 2: Absorbance spectra of iNOSoxy. The thick line spectrum is 2 μM iNOSoxy in the presence of 0.5 mM $5MeH_4B$ and DTT. The thin line spectrum was recorded 20 min after subsequent addition of 0.2 mM Arg.

hyde for precolumn derivatization (*4*). For radioisotope detection, 10 μM iNOSoxy was incubated with 0.6 mM $5MeH_4B$ or 0.2 mM H_4B, 20 μM [^{14}C]Arg, and 0.23 mM Arg for at least 4 h. UV−vis spectroscopy was used to monitor the completeness of Arg binding as judged by buildup of a heme Soret peak at 395 nm. The solution was made anaerobic, the enzyme reduced by dithionite titration, and 0.2 mL was quickly mixed with 20 μL of O_2-saturated buffer containing 1 mM Arg, 100 μM NOHA, and 100 μM L-citrulline for 10−30 s followed by quenching with 20 μL of quenching buffer (2 N HCl in 50% 2-propanol). Sample workup, separation on cation HPLC, and quantitation were done as described previously (*19*).

Crystallization. Murine iNOSoxyΔ65 (residues 66−498) was overexpressed and purified for crystallization as described previously (*33*, *37*). Crystals were grown at 4 °C using the hanging drop method. The iNOSoxy concentration was 25 mg/mL in 40 mM EPPS (pH 7.6) containing 4 mM $5MeH_4B$ and 3 mM AR-C95791AA, an N-substituted aminopyridine NOS inhibitor, supplied by AstraZeneca. This inhibitor improves NOSoxy crystal stability and diffraction quality (details of AR-C95791AA interactions in the substrate binding site of NOS to be published elsewhere). The reservoir contained 26% $LiSO_4$, 100 mM MES (pH 5.3), and 50 mM BOG. A total of 2.5 μL of protein was mixed with an equal volume of reservoir, and crystals were grown in 1−2 days. Diffraction data were collected at the Stanford Synchrotron Radiation Laboratory (SSRL) on beamline 7-1 at −170 °C. DENZO (*30*) was used to process the data. The initial model was obtained from the iNOSoxy plus H_4B structure (*7*). CNS (*31*) was used for crystallographic refinement, and TURBO−FRODO (*32*) was used for electron density map fitting.

RESULTS

We used UV−vis spectroscopy to determine conditions required to bind $5MeH_4B$ to iNOSoxy. In the absence of Arg and $5MeH_4B$, the iNOSoxy dimer had DTT bound to its heme as judged by its split Soret absorbance at 395 and 475 nm (not shown), consistent with previous results (*28*). When $5MeH_4B$ was added to the protein at 0.5 mM (Figure 2) or incubated with the protein overnight (not shown) it was unable to displace DTT, although H_4B displaces DTT under these conditions (*28*). This suggests that $5MeH_4B$ when added alone does not bind to iNOSoxy. However, when 0.2 mM Arg was added to the mixture of iNOSoxy plus $5MeH_4B$ it caused displacement of bound DTT within 20 min as judged by appearance of a new Soret peak at 395 nm (Figure 2). Because Arg when added alone displaces DTT much more slowly from iNOSoxy (*33*), this result indicated that $5MeH_4B$ can bind to iNOSoxy in the presence of Arg. This is consistent with H_4B and Arg binding to full-length iNOS in a cooperative manner (*33*, *34*).

We next ran single catalytic turnover reactions at 10 °C by ferrous iNOSoxy that contained Arg plus $5MeH_4B$. Anaerobic protein solutions were rapidly mixed with an O_2-containing buffer to initiate the reactions. They were then analyzed by rapid scanning to follow heme transitions, rapid freezing to follow buildup and decay of the $5MeH_4B$ radical, and rapid quenching to follow product formation from Arg. Results were compared to those obtained in reactions that contained Arg- and H_4B-saturated iNOSoxy run under identical conditions (*19*).

Heme Transitions. Rapid scanning discerned three spectrally distinct species during the single turnover reaction (Figure 3, panel A), whose spectral properties identified them as the beginning ferrous iNOSoxy species, a transient heme $Fe^{III}O_2^-$ intermediate, and ending ferric enzyme species (*19*, *22*). The Soret and visible absorbance peaks of the $Fe^{III}O_2^-$ intermediate were at 425, 554, and 586 nm, respectively, which are highly similar to absorbance features of the $Fe^{III}O_2^-$ intermediate formed in a reaction of iNOSoxy that contains H_4B plus Arg. Global analysis of the spectral data showed that it fit best to an A → B → C kinetic model with monophasic transitions for formation and disappearance of the $Fe^{III}O_2^-$ intermediate. Figure 3, panel B illustrates how the concentrations of the three species changed with time during the single turnover reaction. The observed rate of $Fe^{III}O_2^-$ formation in this circumstance was identical to that obtained in a reaction with iNOSoxy containing H_4B plus Arg (Table 1). However, conversion of the $Fe^{III}O_2^-$ intermediate to ferric enzyme was approximately 3 times faster in the $5MeH_4B$-bound iNOSoxy as compared to the H_4B-bound iNOSoxy (Table 1). Doubling the concentration of $5MeH_4B$ did not alter the kinetics of these transitions, consistent with saturation binding.

To check the accuracy of the global analysis, we plotted actual absorbance values recorded at 427 and 395 nm during the single turnover reaction (Figure 3, panel C). Absorbance at these two wavelengths represents the Soret maximum for the $Fe^{III}O_2^-$ intermediate and the ferric iNOSoxy species, respectively. Absorbance change at each wavelength was biphasic because of O_2 binding to ferrous iNOSoxy in the first 30 ms (*35*). Subsequent absorbance data recorded at either wavelength (from approximately 30 to 280 ms) fit well to a single-exponential equation and thus suggested a monophasic transition without detectable buildup of spectrally distinct intermediates. Rates of absorbance change at 395 and 427 nm during the transition were 30.4 and 29.9 s^{-1}, respectively, which match well to the rates calculated by global analysis (Table 1). Thus, we conclude that $5MeH_4B$ supports faster conversion of the $Fe^{III}O_2^-$ intermediate to ferric enzyme as compared to H_4B during the Arg single turnover reaction catalyzed by iNOSoxy.

Kinetics of Radical Formation and Decay. Rapid-freeze experiments with $5MeH_4B$- and Arg-saturated iNOSoxy protein showed that a free radical signal built up during the

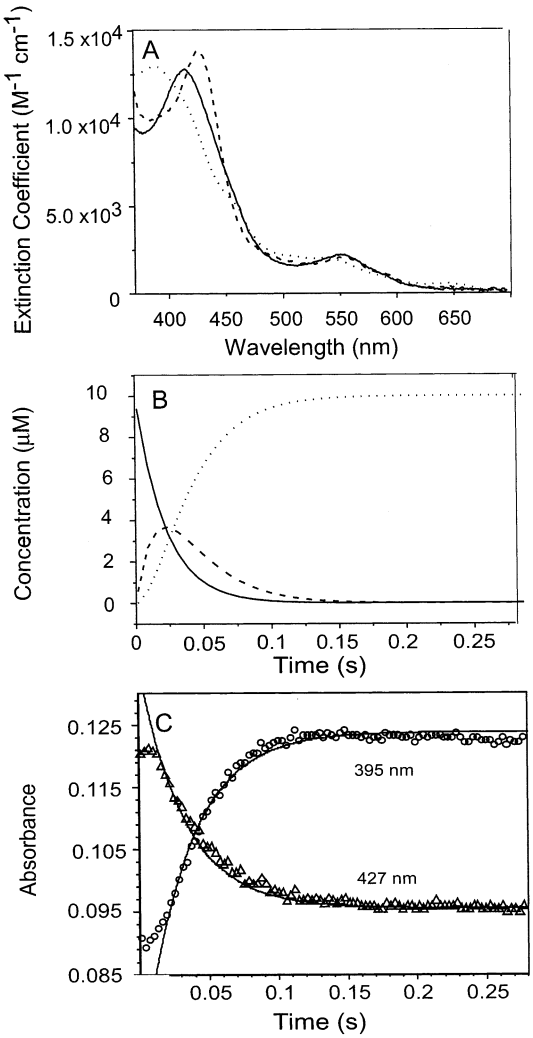

FIGURE 3: Light absorbance spectra and kinetics of heme species present during a single turnover Arg hydroxylation catalyzed by 5MeH$_4$B-containing iNOSoxy. Final enzyme concentration was 10 μM. Panel A, light absorbance spectra for three species discerned by global analysis of the kinetic data: The beginning ferrous iNOSoxy (solid line), a transient $Fe^{III}O_2^-$ intermediate (dashed line), and the final ferric iNOSoxy (dotted line). Panel B, concentrations of these three species vs time of the reaction. Panel C, absorbance values at 427 and 395 nm vs time of the reaction, showing single-exponential line of best fit created with data points recorded at 30 ms and beyond. Data are representative of 3 or 4 independent experiments.

single turnover reactions run at 10 °C. The radical signal was centered at $g = 2.0$, had a peak to trough width of 40 G, and exhibited a $p_{1/2}$ value of 40 mW at 150 °K (Figure 4). These characteristics are highly similar to the H$_4$B radical that forms in iNOSoxy under identical reaction conditions (*19*), although the radical signal formed in the 5MeH$_4$B iNOSoxy reaction had a different hyperfine spectrum as compared to the H$_4$B radical (Figure 4). Changing the measurement temperature did not alter the line shape of the radical signal, and increasing the 5MeH$_4$B concentration 2-fold in the reaction did not change the intensity of the radical signal (data not shown). Together, these data indicate that 5MeH$_4$B forms a radical in iNOSoxy during the Arg single turnover reaction.

Simulations of the H$_4$B and 5MeH$_4$B radicals are shown as the dotted and dashed lines in Figure 4. Hyperfine coupling constants that we obtained from the simulations are summarized in Table 2. In the case of H$_4$B, the simulation that gave the best fit to the data involved two ^{14}N nuclei with (isotropic) splitting of 13.0 and 2.5 G, and three ^{1}H nuclei with (again isotropic) splittings of 14.5, 10, and 5 G.[2] Utilization of additional proton coupling or incorporating anisotropy into the coupling of the three predominant protons did not significantly improve the fit to the data, resulting in only modest line-broadening and no improvement in the low- and high-field shoulders. There was no manifest coupling to the heme, but as previously noted (*23*) proximity to the heme site was reflected in the resistance to power saturation of the pterin radical signal.

Fits of the 5MeH$_4$B spectra required three equivalent ^{1}H nuclei with couplings of 12.5 G rather than the one with 10

Table 1: Data for Arg Single Turnover Reactions Catalyzed by iNOSoxy Containing H$_4$B or 5MeH$_4$B[a]

transformation	H$_4$B	5MeH$_4$B
$Fe^{III}O_2^-$ formation (s^{-1})[b]	52.7 ± 2.2 (4)[c]	52.7 ± 6.0 (4)
$Fe^{III}O_2^-$ disappearance (s^{-1})	12.5 ± 0.2 (4)[c]	34.7 ± 2.2 (4)
NOHA formation (s^{-1})	9.2 ± 1.1 (3)[c]	30 ± 4 (3)
pterin radical formation (s^{-1})	11.1 (2)[c]	40 (2)
pterin radical decay (s^{-1})	0.71 (2)[c]	0.2 (2)
NOHA production per heme	0.61 ± 0.08 (3)[d] 0.57 ± 0.12 (3)[e]	0.84 ± 0.07 (3)[d] 0.73 ± 0.15 (3)[e]

[a] Anaerobic ferrous iNOSoxy that contained Arg (or [^{14}C]Arg) and H$_4$B or 5MeH$_4$B was rapid-mixed with O_2-containing buffer at 10 °C to start the reaction. Subsequent transformations were followed either by stopped-flow rapid-scanning spectroscopy, rapid-quenching and HPLC analysis, or rapid-freezing and EPR spectroscopy. [b] Values are the means ± SD with number of experiments in parentheses. [c] Data from ref *19*. [d] Values obtained from reactions that contained [^{14}C]Arg. [e] Values obtained from reactions that contained Arg at a concentration of 1 mM.

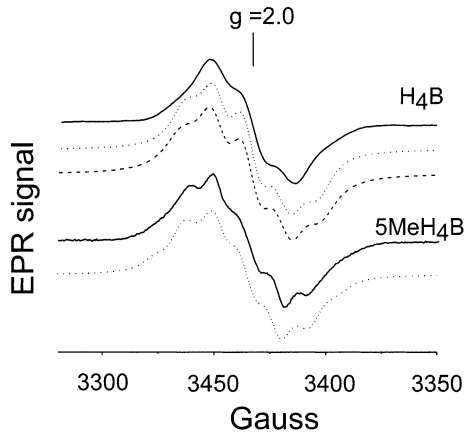

FIGURE 4: Pterin radical signals formed during Arg oxidation by iNOSoxy. Reactions were initiated by rapid mixing O_2-saturated buffer with an anaerobic solution of 0.4 mM ferrous iNOSoxy containing 2.5 mM 5MeH$_4$B and 20 mM Arg. Data shown are from two independent experiments. Data for reactions that contained H$_4$B are taken from ref *19*. Simulated EPR spectra of H$_4$B (5 nucleus, dotted line; 7 nucleus, dashed line) and 5MeH$_4$B radicals (dotted line) were obtained using the xmer program and employing the Monte Carlo method (*50*) and similar parameters used in ref *23*.

[2] We have been unable to reproduce the simulations reported by Schmidt et al. (*23*) using the coupling parameters reported in this work. Our simulations of the H$_4$B radical spectra reported here systematically overemphasize to a certain degree the shoulders on the spectrum that lie to low and high field, as reflected in Figure 4, but nevertheless represent acceptable simulations of the data.

Table 2: Hyperfine Coupling Constants Obtained from Simulation

species	A_I N5	A_I N5-H_α	A_I N5-$CH_{3\beta1}$	A_I N5-$CH_{3\beta2}$	A_I N5-$CH_{3\beta3}$	A_I C6-H_β	A_I N8	A_I N8-H	A_I C7-$H_{\beta1}$	A_I C7-$H_{\beta2}$
H_4B radical (5 nucleus)	13.0	10.0				14.5	2.5	5.0		
H_4B radical (7 nucleus)	13.0	12.0				14.5	1.5	4.5	3.5	2.0
$5MeH_4B$ radical (7 nucleus)	10.0		12.5	12.5	12.5	14.0	3.5	3.3		

G splitting and presumably arise from the three protons of the N5-methyl group. The strength of coupling of the methyl protons is consistent with the majority of the unpaired spin density on the pterin nucleus being largely localized on N5 in the 5-methyl derivative as well as normal H_4B (*36*). Simulations of the $5MeH_4B$ spectrum were not significantly improved by including additional proton coupling in the simulation or by incorporating anisotropy into either the nitrogen or the proton hyperfine coupling, despite the fact that our EPR spectrum exhibited considerably greater fine structure than that reported by Schmidt et al. (*23*). On the basis of the number of proton couplings included in their simulations, a total of five in the case of normal H_4B, those authors conclude that the pterin radical exists as a protonated cation in NOS. Since in our simulations no more than three protons were required to adequately simulate the data, we cannot conclude on the basis of our own data that the pterin radical must be protonated in the signal-giving species. We note that a protonated H_4B radical is expected to be extremely acidic (*36*) and very likely to deprotonate to the neutral radical at pH ~7, the electrostatic interaction with the heme propionate group notwithstanding.

Figure 5A compares buildup and decay kinetics of $5MeH_4B$ and H_4B radical signals during single turnover reactions catalyzed by iNOSoxy at 10 °C. Radical signal intensities were fitted to an A → B → C reaction model to determine formation and decay rates (*22*), using a lag time of 15 ms to account for the time required for O_2 binding to ferrous iNOSoxy heme. The $5MeH_4B$ radical signal achieved a maximum intensity at 60−80 ms as compared to 125 ms for H_4B. The fitting gave rates of formation and decay for the $5MeH_4B$ radical that were 40 and 0.2 s^{-1}, respectively, and indicated that 100% of the bound $5MeH_4B$ participated in radical formation during the reaction. Thus, the $5MeH_4B$ radical formed at a rate that was approximately 4 times faster than the H_4B radical in identical Arg reactions run at 10 °C, and it decayed 3 times more slowly than the H_4B radical (Table 1).

Product Formation Kinetics. Rapid-quench experiments revealed that [^{14}C]Arg conversion to NOHA was 3 times faster in $5MeH_4B$-containing iNOSoxy as compared to an equivalent H_4B-containing enzyme (Figure 5B and Table 1). Other experiments that measured the extent of Arg oxidation showed that iNOSoxy containing $5MeH_4B$ generated 38% more NOHA per heme than an equivalent H_4B-containing enzyme (Table 1). This indicated that faster pterin radical formation in the single turnover reactions is associated with faster and more extensive Arg hydroxylation.

Crystallographic Structure of 5MeH$_4$B-Bound iNOSoxy. To determine if protein structural changes were associated with the kinetic differences that we observed for H_4B substitution with $5MeH_4B$, we determined the crystal structure of a $5MeH_4B$-bound iNOSoxy dimer to 1.8 Å resolution. Crystallographic data collection and refinement statistics are

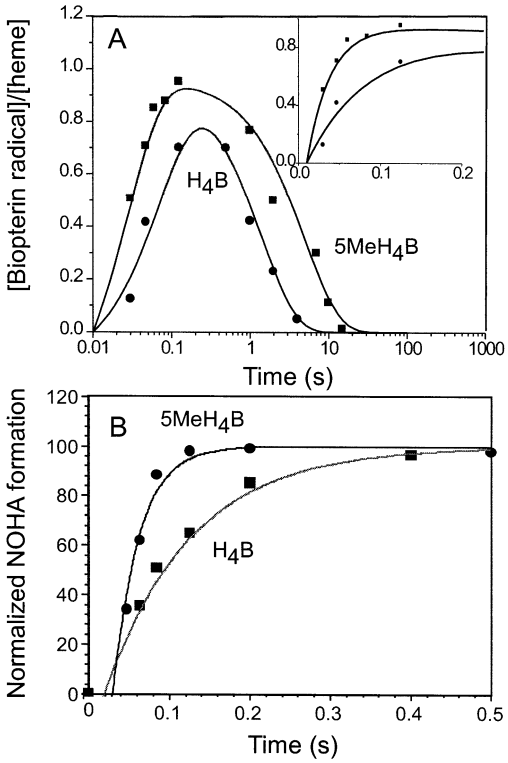

FIGURE 5: Kinetics of pterin radical formation, decay, and product formation during Arg hydroxylation by $5MeH_4B$- or H_4B-saturated iNOSoxy. Reactions were set up and run as described in Figure 4. Panel A shows radical formation and decay vs the log of the reaction time. Inset, radical buildup vs time during the first 130 ms of reaction for iNOSoxy containing $5MeH_4B$ (solid squares) or H_4B (solid circles). Panel B shows the kinetics of NOHA formation. Reactions were initiated by mixing an anaerobic solution of 3 μM ferrous iNOSoxy containing 1 mM $5MeH_4B$ and 10 μM [^{14}C]Arg with air-saturated buffer. Data for H_4B-bound iNOSoxy was taken from ref *19*. The percentage of [^{14}C]Arg conversion to [^{14}C]NOHA was 39% for H_4B-bound iNOSoxy and 10% for $5MeH_4B$-bound iNOSoxy under these experimental conditions. Data are normalized to better compare their time courses and are the representative of three experiments each.

listed in Table 3. The overall structure of the $5MeH_4B$-bound iNOSoxy was almost indistinguishable from iNOSoxy with bound H_4B (*7*, *37*−*39*). The close similarity extends to the pterin ring site, where most of the H-bonding and all of the π stacking interactions between H_4B and the protein residues (*7*) are preserved in the $5MeH_4B$ structure (Figure 6A,B). Hydrogen bonds between the heme propionate and the pterin ring are also maintained bwtween the H_4B-bound and $5MeH_4B$-bound structures. An overlay of these two structures shows only minor differences between them in the conformation, orientation, and position of the pterin and surrounding residues (Figure 6C). The pterin N5 remains tetrahedral, with the added methyl group out of the ring plane. The pterin tilts slightly to avoid a collision of the 5-methyl group with Arg 375. The hydrogen bond from pterin N5 to a structural water molecule is broken, and both this water molecule and

Table 3: Crystallographic Data Collection and Refinement Statistics for 5MeH$_4$B-Containing iNOSoxy

wavelength (Å)	1.08
cell dimensions (Å)	$a = b = 214.16$; $c = 117.65$
data resolution (Å)	30.0−1.8 (1.86−1.80)[a]
total observations	1 279 733
unique observations	142 082
completeness (%)	97.5 (92.4)
$\langle I/\sigma \rangle$[b]	29.6 (4.2)
R_{sym}[c]	0.03 (0.28)
R[d]	0.201
R_{free}[e]	0.216
no. non-hydrogen atoms	7957
no. waters	847
⟨overall B⟩ (Å^2)	29.4
⟨main chain B⟩ (Å^2)	28.7
⟨side chain B⟩ (Å^2)	29.9
rms bond (Å)	0.009
rms angle (deg)	1.4

[a] Highest resolution shell for compiling statistics. [b] Average intensity signal-to-noise ratio. [c] $R_{sym} = \sum\sum_j |I_j - \langle I \rangle| / \sum\sum_j I_j$. [d] $R = \sum ||F_o| - |F_c|| / \sum |F_o|$, where F_o and F_c are the observed and calculated structure factors, respectively. [e] 5% of the reflections were set aside randomly for R_{free} calculation.

a neighboring water molecule adjust their positions to maintain other hydrogen bonds. The tilt of the pterin and shifts in the side chain of Met 114 bring its thiomethyl group slightly closer to the pterin ring (Figure 7). Overall, these subtle structural changes imply that 5MeH$_4$B binds without significant differences in its conformation or in the conformation of the surrounding protein relative to H$_4$B-bound iNOSoxy.

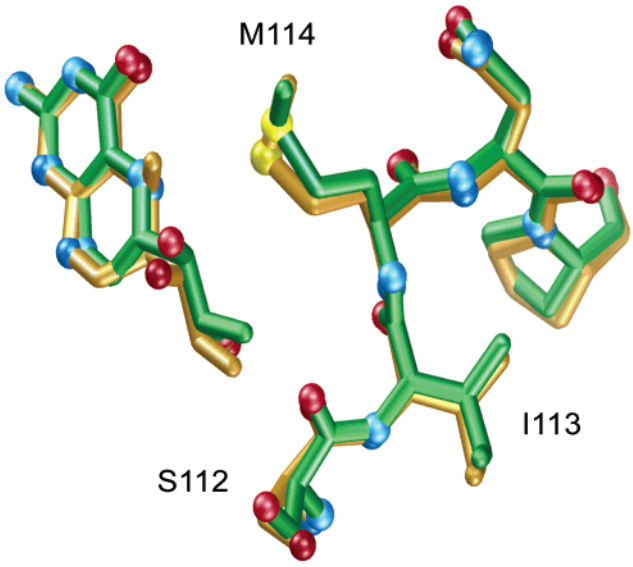

FIGURE 7: Pterin dihydroxypropyl side chain binding environment in H$_4$B-bound and 5MeH$_4$B-bound iNOSoxy. The figure overlays structures for the H$_4$B (green) and 5MeH$_4$B (yellow) bound iNOSoxy. The sulfur atom of Met114 is yellow. Water molecules and hydrogen bonds are omitted for clarity.

DISCUSSION

H$_4$B reduces a transient $Fe^{III}O_2^-$ intermediate to create the ultimate heme−oxy species that hydroxylates Arg (Figure 1). Here, we show that modifying the structure of H$_4$B alters the kinetics of its electron transfer to the $Fe^{III}O_2^-$ intermediate. Our stopped-flow UV−vis and rapid freeze EPR experiments suggest that 5MeH$_4$B reduces the $Fe^{III}O_2^-$ intermediate about 4 times faster than does H$_4$B. This complements our previous finding that Trp457 in iNOSoxy also controls the speed of this electron transfer (*22*). Thus, both the pterin structure and the surrounding protein environment can tune electron transfer from H$_4$B.

Faster 5MeH$_4$B radical formation was associated with faster conversion of the $Fe^{III}O_2^-$ intermediate to ferric enzyme and with faster Arg hydroxylation. A kinetic match among these three processes had also been observed in reactions catalyzed by H$_4$B-containing wild-type iNOSoxy and for the W457A and W457F mutants (*19*, *22*). In those studies, the mutants had slower H$_4$B radical formation that was associated with slower $Fe^{III}O_2^-$ disappearance and slower Arg hydroxylation. Our current data extend these results by showing that kinetic matching is still maintained among these processes even when pterin radical formation becomes 4-fold faster than that observed with H$_4$B.

Equivalent rates of Arg hydroxylation and 5MeH$_4$B radical formation suggest that the latter process is still rate limiting for the single turnover reaction. This is consistent with our observing no spectral intermediates during conversion of the

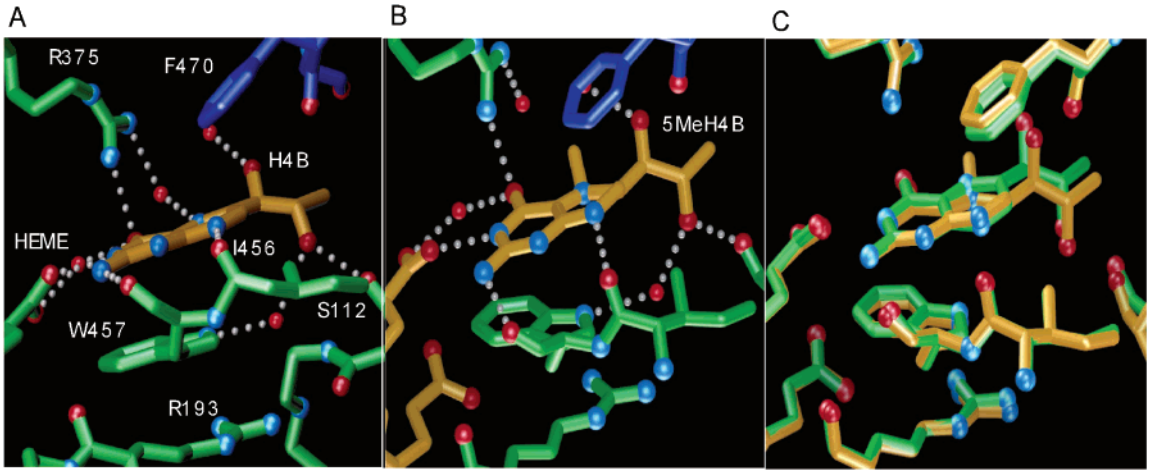

FIGURE 6: Comparison of pterin ring binding sites in H$_4$B-bound and 5MeH$_4$B-bound iNOSoxy. In Panels A and B, the bound pterin is yellow and is surrounded by green and blue residues from the same or partner subunit of the dimer, respectively. Hydrogen bonds are shown as white dotted lines, oxygen atoms are red, while nitrogen atoms are blue. Panel C shows a superimposition of the H$_4$B-bound (green) and 5MeH$_4$B-bound (yellow) iNOSoxy. Water molecules and hydrogen bonds are omitted for clarity.

$Fe^{III}O_2^-$ intermediate to ferric enzyme in $5MeH_4B$-saturated iNOSoxy. If reaction steps downstream from $5MeH_4B$ electron transfer had become rate limiting, we should have observed a slower rate of Arg hydroxylation and possibly observed buildup of new spectral intermediates. Thus, we conclude that subsequent steps in the iNOSoxy reaction that follow $Fe^{III}O_2^-$ reduction by $5MeH_4B$ (i.e., formation of the ultimate heme-based oxidant and its reaction with Arg) likely proceed at similar or greater speed than $5MeH_4B$ radical formation (30 s^{-1} at 10 °C). To observe these steps, we may need to find a H_4B analogue that supports even faster $Fe^{III}O_2^-$ reduction or engineer the protein to receive electrons through a pulse laser step (*40*).

The extent of Arg hydroxylation per heme was 28−37% greater in $5MeH_4B$-saturated iNOSoxy as compared to the H_4B-saturated enzyme. We previously observed that slower $Fe^{III}O_2^-$ reduction by H_4B was associated with proportionally less Arg hydroxylation in W457 mutants (*22*). Indeed, the rank orders of $Fe^{III}O_2^-$ reduction rate and product yield are the same ($5MeH_4B$ > H_4B > H_4B/W457F > H_4B/W457A). This relationship between kinetics and product yield can be rationalized if one considers that the speed of $Fe^{III}O_2^-$ reduction by H_4B controls partitioning of this intermediate between productive (Arg hydroxylation) versus nonproductive (superoxide release) pathways (*20*). Thus, greater product yield with $5MeH_4B$ may reflect its ability to shift a higher percentage of the $Fe^{III}O_2^-$ intermediate toward Arg hydroxylation. This relationship underscores the need for timely $Fe^{III}O_2^-$ reduction in iNOS. Moreover, it helps rationalize why H_4B provides an electron at this step instead of the NOS flavoprotein domain, whose electron transfer to heme is slower in iNOS (approximately 1 s^{-1}) (*26*).

The driving force for electron transfer between H_4B and the $Fe^{III}O_2^-$ intermediate is determined in part by the redox couples of the two participating species. Although midpoint potential values for H_4B and the $Fe^{III}O_2^-$ intermediate have not been measured in any NOS, some related information is available. Gorren et al. (*41*) utilized cyclic and square wave voltammetry to study oxidative transitions of various reduced pterins in solution at neutral pH. One-electron oxidative transitions for H_4B and $5MeH_4B$ were observed at +270 and +400 mV, respectively. Because these values are far more positive than midpoint potentials estimated for a heme−thiolate $Fe^{III}O_2^-$ intermediate (−300 to 10 mV) (*42*−*44*), the NOS protein may perturb bound H_4B to increase its reducing power. Flavoproteins provide a good precedent for this effect because they can perturb the hydroquinone−semiquinone midpoint potential of a single bound flavin over an approximate 400 mV range (*45*). In a related study[3], we have observed that binding $5MeH_4B$ lowers the ferric heme midpoint potential of an Arg-bound iNOSoxy by about 40 mV, which is a slightly greater negative change than what we obtained using H_4B in the same circumstance (*46*). On the other hand, if oxidation of Arg is fast and irreversible it may overcome the reversible and unfavorable electron-transfer step from the pterin. It will be important to study how NOS proteins tune the midpoint potential of H_4B and understand what other factors promote its electron transfer to the $Fe^{III}O_2^-$ intermediate.

[3] Santolini, J., and Stuehr, D. J., unpublished results.

In principle, the different rates of $5MeH_4B$ and H_4B radical formation should relate to their different chemical structures and/or to distinct changes in iNOSoxy structure once either pterin is bound. Crystal structures suggest that bound H_4B may be stabilized within NOSoxy as a cation radical during turnover by an extensive hydrogen bonding network (*8*, *24*, *37*). The positive charge is thought to localize predominantly at the N5 position in H_4B (*37*) and to be additionally stabilized by a cation−π cloud interaction that is contributed in iNOSoxy by conserved aromatic residues W457 and F470 (*24*). Importantly, the H_4B radical has also been proposed to be cationic with radical density primarily located at N5 of the biopterin ring as judged from ^{15}N isotope substitution and other EPR experiments (*21*, *23*). This radical density assignment is consistent with our EPR data since methyl group substitution at N5 changed the hyperfine fingerprint as compared to the H_4B radical (Figure 4). Given these circumstances, adding a methyl group at N5 should further stabilize the radical and thus facilitate its formation during Arg hydroxylation.

Regarding protein interactions with $5MeH_4B$, our crystal structure suggests that there are no significant differences between iNOSoxy proteins containing $5MeH_4B$ versus H_4B. The hydrogen bonding and π stacking interactions between bound cofactors and the surrounding amino acids are very similar. Relative to H_4B in iNOSoxy, $5MeH_4B$ is slightly tilted to accommodate the added methyl group. Two structural water molecules shift to improve packing with the methylated H_4B, but one of these loses a hydrogen bond to N5. The thiomethyl of Met 114 packs more closely with $5MeH_4B$, but no conformational strain in $5MeH_4B$ is evident from the crystal structure. Thus, faster radical formation by $5MeH_4B$ is not linked to obvious changes in protein structure or interactions. This contrasts with the iNOSoxy W457A and W457F mutants, whose slower H_4B radical formation is linked to discrete structural changes in their H_4B binding sites that may destabilize the cation radical (*22*, *24*).

The half-lives of radicals in our iNOSoxy reactions were much longer than the half-life of an H_4B radical formed in solution at neutral pH (*47*, *48*). Thus, iNOSoxy appears to stabilize the H_4B radical after it forms during Arg hydroxylation. This is important because delaying its oxidation would give the enzyme time to reduce the radical back to H_4B, which must occur before the second step of NO synthesis can be initiated (*4*, *5*).

Although we do not know with certainty the fate of the pterin radical in our experiments, we and other groups have argued that the pterin radical is likely to become oxidized following completion of the single turnover reaction. This assumption is consistent with the pterin radical being inherently unstable in the presence of O_2 (and so eventually must oxidize according to the thermodynamics). Also, there are no obvious reducing agents present in our reactions to transform the pterin radical back into its fully reduced form. We do not expect that disappearance of the radical is connected to pterin dissociation from NOS, as binding studies (*33*) and multiple turnover experiments have clearly indicated that enzyme affinity for H_4B and its radical are high enough to keep them bound during multiple rounds of catalysis.

Stabilizing the H_4B radical may also be a fundamental means for regulating H_4B electron-transfer rate in iNOSoxy. A synthesis of our current and previous work reveals a direct

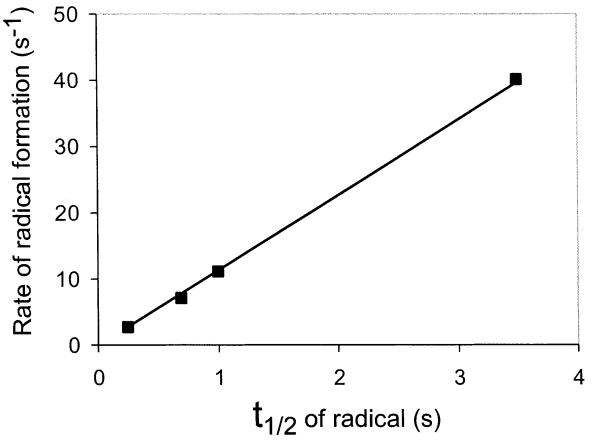

FIGURE 8: Correlation between rate of pterin radical formation during Arg hydroxylation and radical half-life in iNOSoxy. Data points (from left to right) represent reactions using W457A, W457F, and wild-type iNOSoxy plus H_4B and wild-type iNOSoxy plus $5MeH_4B$. The W457 mutant data is from ref *22*.

correlation between H_4B radical half-life and the rate at which it forms in iNOSoxy (Figure 8). These data predict that the speed of H_4B radical formation is equivalent to the radical half-life multiplied by a factor of 11. The degree of correlation is remarkable given that radical half-life was altered by mutating the protein in two cases (W457A and F) and by modifying H_4B structure in one case. To the best of our knowledge, this is the first example where the rate of radical formation in a protein has been directly related to the stability of the resulting radical. It will be interesting to investigate the basis for this relationship and to see if it holds in other NOS isozymes.

ACKNOWLEDGMENT

We thank AstraZeneca for AR-C95791AA. We thank Abby Meade and John McDonald for protein purification and Mika Aoyagi for help in generating the crystallographic illustrations.

REFERENCES

1. Alderton, W. K., Cooper, C. E., and Knowles, R. G. (2001) *Biochem. J. 357*, 593−615.
2. Roman, L. J., Martásek, P., and Masters, B. S. (2002) *Chem. Rev. 102*, 1179−1190.
3. Stuehr, D. J., and Ghosh, S. (2000) in *Handbook of Experimental Pharmacology* (Mayer, B., Ed.), pp 33−70, Springer-Verlag, Berlin.
4. Boggs, S., Huang, L., and Stuehr, D. J. (2000) *Biochemistry 39*, 2332−2339.
5. Bec, N., Gorren, A. C., Voelker, C., Mayer, B., and Lange, R. (1998) *J. Biol. Chem. 273*, 13502−13508.
6. Hurshman, A. R., and Marletta, M. A. (2002) *Biochemistry 41*, 3439−3456.
7. Crane, B. R., Arvai, A. S., Ghosh, D. K., Wu, C., Getzoff, E. D., Stuehr, D. J., and Tainer, J. A. (1998) *Science, 279*, 2121−2126.
8. Raman, C. S., Li, H., Martasek, P., Kral, V., Masters, B. S., and Poulos, T. L. (1998) *Cell 95*, 939−950.
9. Fischmann, T. O., Hruza, A., Niu, X. D., Fossetta, J. D., Lunn, C. A., Dolphin, E., Prongay, A. J., Reichert, P., Lundell, D. J., Narula, S. K., and Weber, P. C. (1999) *Nat. Struct. Biol. 6*, 233−242.
10. Gachhui, R., Abu-Soud, H. M., Ghosha, D. K., Presta, A., Blazing, M. A., Mayer, B., George, S. E., and Stuehr, D. J. (1998) *J. Biol. Chem. 273*, 5451−5454.
11. Adak, S., Santolini, J., Tikunova, S., Wang, Q., Johnson, J. D., and Stuehr, D. J. (2001) *J. Biol. Chem. 276*, 1244−1252.
12. Miller, R. T., Martasek, P., Omura, T., and Siler Masters, B. S. (1999) *Biochem. Biophys. Res. Commun. 265*, 184−188.
13. Sato, H., Sagami, I., Daff, S., and Shimizu, T. (1998) *Biochem. Biophys. Res. Commun. 53*, 845−849.
14. Sono, M., Stuehr, D. J., Ikeda-Saito, M., and Dawson, J. H. (1995) *J. Biol. Chem. 270*, 19943−19948.
15. Gorren, A. C., Bec, N., Schrammel, A., Werner, E. R., Lange, R., and Mayer, B. (2000) *Biochemistry 39*, 11763−11708.
16. Couture, M., Stuehr, D. J., and Rousseau, D. L. (2000) *J. Biol. Chem. 275*, 3201−3205.
17. Adak, S., Wang, Q., and Stuehr, D. J. (2000) *J. Biol. Chem. 275*, 33554−33561.
18. Rusche, K. M., Spiering, M. M., and Marletta, M. A. (1998) *Biochemistry 37*, 15503−15512.
19. Wei, C. C., Wang, Z. Q., Wang, Q., Meade, A. L., Hemann, C., Hille, R., and Stuehr, D. J. (2001) *J. Biol. Chem. 276*, 315−319.
20. Stuehr, D., Pou, S., and Rosen, G. M. (2001) *J. Biol. Chem. 276*, 14533−14536.
21. Hurshman, A. R., Krebs, C., Edmondson, D. E., Huynh, B. H., and Marletta, M. A. (1999) *Biochemistry 38*, 15689−15696.
22. Wang, Z. Q., Wei, C. C., Ghosh, S., Meade, A. L., Hemann, C., Hille, R., and Stuehr D. J. (2001) *Biochemistry 40*, 12819−12825.
23. Schmidt, P. P., Lange, R., Gorren, A. C., Werner, E. R., Mayer, B., and Andersson, K. K. (2001) *J. Biol. Inorg. Chem. 6*, 151−158.
24. Aoyagi, M., Arvai, A. S., Ghosh, S., Stuehr, D. J., Tainer, J. A., and Getzoff, E. D. (2001) *Biochemistry 40*, 12826−12832.
25. Werner, E. R., Habisch, H. J., Gorren, A. C., Schmidt, K., Canevari, L., Werner-Felmayer, G., and Mayer, B. (2000) *Biochem. J. 348*, 579−583.
26. Presta, A., Siddhanta, U., Wu, C., Sennequier, N., Huang, L., Abu-Soud, H. M., Erzurum, S., and Stuehr, D. J. (1998) *Biochemistry 37*, 298−310.
27. Kotsonis, P., Frohlich, L. G., Raman, C. S., Li, H., Berg, M., Gerwig, R., Groehn, V., Kang, Y., Al-Masoudi, N., Taghavi-Moghadam, S., Mohr, D., Munch, U., Schnabel, J., Martasek, P., Masters, B. S., Strobel, H., Poulos, T., Matter, H., Pfleiderer, W., and Schmidt, H. H. (2001) *J. Biol. Chem. 276*, 49133−49141.
28. Ghosh, S., Wolan, D., Adak, S., Crane, B. R., Kwon, N. S., Tainer, J. A., Getzoff, E. D., and Stuehr, D. J. (1999) *J. Biol. Chem. 274*, 24100−24112.
29. Stankovich, M. T. (1980) *Anal. Biochem. 109*, 295−308.
30. Otwinowski, Z., and Minor, W. (1997) *Methods Enzmol. 276*, 307.
31. Brunger, A. T., Adams, P. D., Clore, G. M., Delano, W. L., Gros, P., Grosse-Kunstleve, R. W., Jiang, J. S., Kuszewski, J., Nilges, N., Pannu, N. S., Read, R. J., Rice, L. M., Simonson, T., and Warren, G. L. (1998) *Acta Crystallogr. D54*, 905−921.
32. Roussel, A., and Cambillau, C. (1989) *Silicon Graphics Geometry Partners Directory* 77−78.
33. Ghosh, D. K., Wu, C., Pitters, E., Moloney, M., Werner, E. R., Mayer, B., and Stuehr, D. J. (1997) *Biochemistry 36*, 10609−10619.
34. Mayer, B., Wu, C., Gorren, A. C., Pfeiffer, S., Schmidt, K., Clark, P., Stuehr, D. J., and Werner, E. R. (1997) *Biochemistry 36*, 8422−8427.
35. Abu-Soud, H. M., Gachhui, R., Raushel, F. M., and Stuehr, D. J. (1997) *J. Biol. Chem. 272*, 17349−17353.
36. Ehrenberg, A., Hemmerich, P., Müller, F., and Pfleiderer, W. (1970) *Eur. J. Biochem. 16*, 584−591.
37. Crane, B. R., Arvai, A. S., Ghosh, S., Getzoff, E. D., Stuehr, D. J., and Tainer, J. A. (2000) *Biochemistry 39*, 4608−4621.
38. Crane, B. R., Rosenfeld, R. J., Arvai, A. S., Ghosh, D. K., Ghosh, S., Tainer, J. A., Stuehr, D. J., and Getzoff, E. D. (1999) *EMBO J. 18*, 6271−6281.
39. Rosenfeld, R. J., Garcin, E. D., Panda, K., Andersson, G., Aberg, A., Wallace, A. V., Morris, G. M., Olson, A. J., Stuehr, D. J., Tainer, J. A., and Getzoff, E. D. (2002) *Biochemistry 41*, 13915−13925.
40. Wang, K., Mei, H., Geren, L., Miller, M. A., Saunders, A., Wang, X., Waldner, J. L., Pielak, G. J., Durham, B., and Millett, F. (1996) *Biochemistry 35*, 15107−15119.
41. Gorren, A. C., Kungl, A. J., Schmidt, K., Werner, E. R., and Mayer, B. (2001) *Nitric Oxide 5*, 176−186.
42. Korth, H.-G., Sustmann, R., Thater, C., Butler, A. R., and Ingold, K. U. (1994) *J. Biol. Chem. 269*, 17776−17779.
43. Groves, J. T., and Wang, C. C−Y. (2000) *Curr. Opin. Chem. Biol. 4*, 687−695.

44. Zhang, Z., Nassar, A.-E. F., Lu, Z., Shenkman, J. B., and Rusling, J. F. (1997) *J. Chem. Soc., Faraday Trans. 93*, 1769−1774.
45. Ludwig, M. L., and Luschinsky, C. L. (1992) in *Chemistry and Biochemistry of Flavoenzymes* (Muller, F., Ed.) Vol. III, p 427−466, CRC Press, Boca Raton, FL.
46. Presta, A., Weber-Main, A. M., Stankovich, M. T., and Stuehr, D. J. (1998) *J. Am. Chem. Soc. 120*, 9560−9465.
47. Patel, K. B., Stratford, M. R. L., Wardman, P., and Everett, S. A. (2002) *Free Radical Biol. Med. 32*, 203−211.
48. Vasquez-Vivar, J., Whitsett, J., Martasek, P., Hogg, N., and Kalyanaraman, B. (2001) *Free Radical Biol. Med. 31*, 975−985.
49. Davydov, R., Ledbetter-Rogers, A., Martasek, P., Larukhin, M., Sono, M., Dawson, J. H., Masters, B. S. S. M., and Hoffman, B. M. (2002) *Biochemistry 41*, 10375−10381.
50. Eloranta, J. (2000) ftp://EPR.chem.jyu.fi/pub/xemr.

BI026898H